Energy Technology
Generation, Conversion, Storage, Distribution
www.entechnol.de

Highly Reversible Phase Transition Endows V_6O_{13} with Enhanced Performance as Aqueous Zinc-Ion Battery Cathode

Lutong Shan, Jiang Zhou, Wanying Zhang, Chengtao Xia, Shan Guo, Xuemei Ma, Guozhao Fang, Xianwen Wu, and Shuquan Liang**

Aqueous zinc-ion batteries (ZIBs), with favorable merits of high security and low cost, have gained much interest in the energy storage field. However, their development is still in its infancy. Herein, V_6O_{13} is investigated as aqueous ZIB cathodes with excellent Zn^{2+} storage performance, as compared with VO_2 and V_2O_5. The intrinsic open structure of V_6O_{13} with mixed-valance states of vanadium (V^{4+}/V^{5+}) is favorable to enable fast Zn^{2+} ion diffusion and improved electronic conductivity, outperforming VO_2 and V_2O_5. Significantly, the highly reversible phase transition of zinc vanadate ($Zn_{0.25}V_2O_5{\cdot}H_2O$) can be detected during discharging, which enables the insertion of more Zn^{2+} ions into the host structure. As a result, V_6O_{13} can exhibit enhanced electrochemical properties, including high capacity and excellent long-term cyclability (206 mA h g^{-1} at 10 A g^{-1} after 3000 cycles).

1. Introduction

The global battery market has been predominated by lithium-ion batteries (LIBs) for dozens of years. Nonetheless, their wide application for the grid-scale field is plagued by the intrinsic drawbacks of high cost and security issues,[1–5] which motivates the development of alternative battery systems. Among the advanced rechargeable battery chemistries, aqueous zinc-ion batteries (ZIBs) have attracted much attention in recent years due to the Zn anode features: abundant resources, high theoretical specific capacity (819 mA h g^{-1}), high redox potential (−0.76 V vs standard hydrogen electrode [SHE]), and multivalent charge carrier.[6–9] In addition, the aqueous system is advantageous for its high safety and low cost, which is of significance for the large-scale application in the energy storage system.[10]

Recently, much effort has been devoted to investigate cathode materials targeting enhanced electrochemical behavior, especially in vanadium-based[6,11–16] and manganese-based materials.[17–22] Nevertheless, it is worthy to note that the research of aqueous ZIBs is still in its infancy, and something is still unclear and debatable with regard to their Zn^{2+} storage mechanism. For instance, the dominated Zn^{2+} insertion/extraction process has been universally illustrated in some vanadium oxides and vanadates,[6,11–13,23–29] while Niu and co-workers demonstrated the simultaneous Zn^{2+} and H^+ insertion in the aqueous $Zn/NaV_3O_8{\cdot}H_2O$ batteries.[15] On the basis of the aqueous Zn/MnO_2 system, Kang and co-workers identified the insertion type of MnO_2 cathode,[17] while a chemical conversion reaction was detected by Liu and co-workers [19] The Zn^{2+} storage/release behavior of aqueous ZIBs is critical for their electrochemical behavior; thus, it is significant to execute scientific and systematic research to explore the advanced storage mechanism targeting outstanding performance.

As is well known, there are several valence states of V in vanadium oxides (mainly V^{3+}, V^{4+}, and V^{5+}), and recent studies have witnessed a series of investigations on vanadium oxides as cathodes in aqueous ZIBs, for example, V_2O_5 and VO_2.[10–12,16,30] The layered structure of V_2O_5 is composed of interconnected VO_5 pyramids that share edges and corners, with the van der Waals forces solely linking the layers (Figure 2a).[31,32] However, V_2O_5 suffers from the dramatic capacity deterioration on account of its inferior electronic conductivity, sluggish diffusion of ions, and terrible structural reversibility.[33] While VO_2 is made up of distorted octahedral VO_6 units based on the oxygen body-centered structure, vanadium atoms locate at the octahedral sites, with octahedral oxygen crystalline sharing both corners and edges, displaying the tunneled structure (Figure 2b).[34] VO_2 possesses a remarkable host framework for rapid Zn^{2+} (de)intercalation, demonstrating excellent rate performance as aqueous ZIB cathodes.[11] Nonetheless, its long-term cycling performance still remains a challenge for widespread applications. Remarkably,

L. Shan, Prof. J. Zhou, W. Zhang, C. Xia, S. Guo, X. Ma, G. Fang, Prof. S. Liang
School of Materials Science and Engineering
Central South University
Changsha 410083, P. R. China
E-mail: zhou_jiang@csu.edu.cn; lsq@csu.edu.cn

Prof. X. Wu
School of Chemistry and Chemical Engineering
Jishou University
Jishou 416000, P. R. China

Prof. J. Zhou, Prof. S. Liang
Key Laboratory of Electronic Packaging and Advanced Functional Materials of Hunan Province
Central South University
Changsha, Hunan 410083, P. R. China

The ORCID identification number(s) for the author(s) of this article can be found under https://doi.org/10.1002/ente.201900022.

DOI: 10.1002/ente.201900022

 © 2019 WILEY-VCH Verlag GmbH & Co. KGaA, Weinheim

with the mixed vanadium states of V^{4+}/V^{5+}, the tunnel-like V_6O_{13} comprises alternative single and double vanadium oxide layers with shared corners, providing more active sites for ion storage,[35,36] during which the sites in double layers are occupied by both VO_6 units with V^{5+} and V^{4+}, while the sites in single layers belong to the VO_6 units with V^{5+} (Figure 2c).[37] Note that V_6O_{13} with alternative single/double layers can be regarded as the combination of single-layered V_2O_5 and double-layered VO_2 with shared corners.[35,38] The advantage of open structure, accompanied by high contents of V^{4+}/V^{5+}, endows V_6O_{13} with the capability of accommodating up to eight Li^+ and delivering a remarkable capacity of 420 mA h g^{-1} and the energy density of 900 W h kg^{-1}, as well illustrated in LIBs.[35,39] Nevertheless, the research on the V_6O_{13} cathode in aqueous ZIBs has not been explored. Herein, we prepared the V_6O_{13} material and employed it as the cathode in aqueous ZIBs, as compared to VO_2 and V_2O_5, which demonstrates excellent electrochemical behavior and undergoes the reversible phase transition process during Zn^{2+} ion insertion/extraction.

2. Results and Discussion

As shown in **Figure 1**, a number of techniques have been devoted to assess the phase and morphology of the V_6O_{13} product. As depicted in Figure 1a, most of the peaks are highly consistent with the standard V_6O_{13} phase (PDF#27-1318). Note that the peaks located at 13.63° and 44.44° can be ascribed to the formation of a small quantity of V_4O_9 (PDF#24-1391) and VO_2 (PDF#71-0565), respectively. From Figure 1b, the V_6O_{13} product features an ultra-thin nanosheet morphology, which is favorable to provide a large contact area and shorten the ion diffusion distance. Moreover, the high-resolution transmission electron microscopy (HRTEM) image accompanied by the consistent selected area electron diffraction (SAED) pattern in Figure 1c further suggests that V_6O_{13} has been successfully synthesized.

The electrochemical behaviors are displayed in **Figure 2**d–f and Figure S1, Supporting Information. Remarkably, V_6O_{13} exhibits higher Zn^{2+} ion diffusion coefficient, better electronic conductivity, and enhanced cycling performance, superior to those of both V_2O_5 and VO_2, rendering it a promising cathode in aqueous ZIBs. From Figure 2e and Table S2, Supporting Information, we can observe that V_6O_{13} presents the charge transfer (R_{ct}) resistance of 590.6 Ω, which is much lower than that of V_2O_5 (1043 Ω) and VO_2 (1261 Ω), as simulated according to previous reports.[40,41] This fact could be attributed to the better electroconductivity of V_6O_{13} resulted from mixed-valence states.[42,43] And it is worthy to note that V_6O_{13} exhibits a metallic character at room temperature,[39] which is also beneficial to its lower R_{ct} value. As can be observed in Figure S2 and Table S3, Supporting Information, the electrochemical impedance spectroscopy (EIS) results of different cycles manifest a significant decrease upon cycling, which could be attributed to the formation of the solid electrolyte interphase and the electrode/electrolyte activation process.[44–46] Different from the previously established Zn^{2+} storage mechanism in vanadium oxides, a highly reversible phase transition ($Zn_{0.25}V_2O_5{\cdot}H_2O$) process can be clearly identified in aqueous Zn/V_6O_{13} system, which endows vanadium oxide with superior electrochemical behavior (206 mA h g^{-1} at 10 A g^{-1} after 3000 cycles).

To investigate the Zn^{2+} storage properties of the as-prepared V_6O_{13} product, we conducted an in-depth electrochemical characterization, as shown in **Figure 3**. The cyclic voltammetry (CV) profiles in Figure 3a manifest several reduction peaks located at 0.55, 0.70, 0.86, and 0.95 V and the oxidation peaks at 0.64, 0.79, 1.01, and 1.09 V, demonstrating the multiple insertion/extraction process of Zn^{2+} storage in V_6O_{13}. It can be observed that the first CV curve displays some variation when compared to the latter curves, which could be due to the activation process.[16,47] The V_6O_{13} electrode demonstrates excellent rate performance (Figure 3b,c) up to 10 A g^{-1}. More significantly, the V_6O_{13} electrode outputs an extraordinary long-term cyclability at the high current density, as observed in Figure 2f and 3d. Notably, it can maintain a high capacity of 295 mA h g^{-1} after 1000 cycles at 5 A g^{-1} and 206 mA h g^{-1} after 3000 cycles at 10 A g^{-1}. It should be pointed out that V_6O_{13} manifests a better, comprehensive electrochemical performance than most previously reported cathode materials in aqueous ZIBs (details in Table S1, Supporting Information), which represents a remarkable advance of aqueous ZIBs cathode materials. It can be observed that the V_6O_{13} material undergoes a rapid capacity decay in the initial stage, which is common in many previous reports.[16,19,24] The phenomenon could mainly be attributed to two factors: for one thing, a little part of inserted Zn^{2+} ions is located at the "dead Zn^{2+} sites" and could not be extracted during the following charge process, resulting in a not-completely reversi-

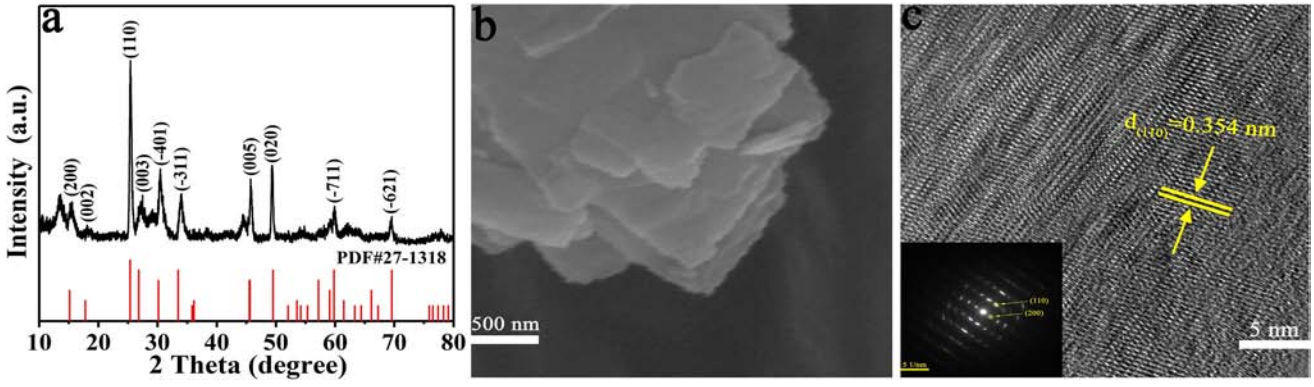

Figure 1. a) XRD pattern, b) SEM image, c) HRTEM image and the corresponding SAED pattern of the V_6O_{13} product.

© 2019 WILEY-VCH Verlag GmbH & Co. KGaA, Weinheim

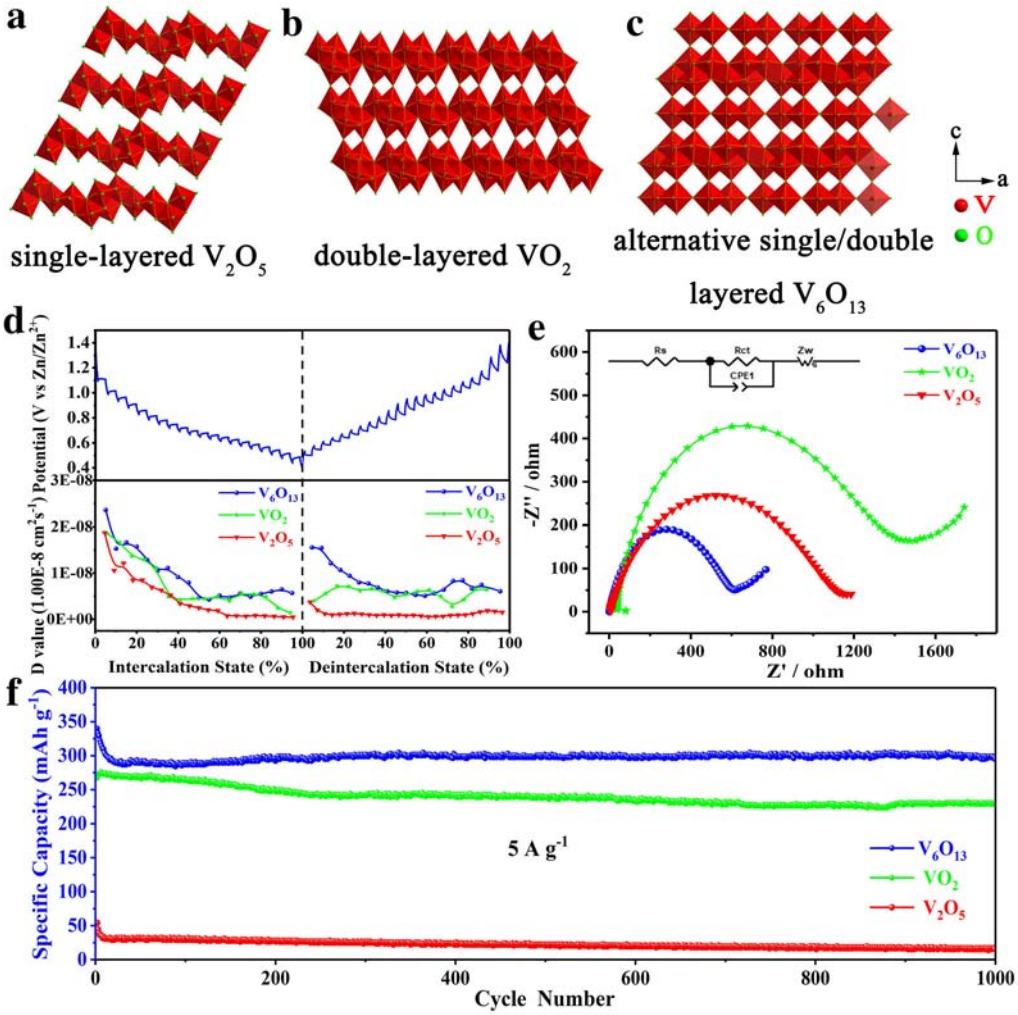

Figure 2. The crystal structures of a) V_2O_5, b) VO_2, and c) V_6O_{13}; d) the discharge–charge galvanostatic intermittent titration technique (GITT) curves of V_6O_{13} and the comparison of zinc-ion coefficient, e) EIS results, and f) long-term cycling performance at 5 A g^{-1} of V_6O_{13}, VO_2, and V_2O_5.

ble de-intercalation process, which can be revealed in the high-resolution X-ray photoelectron spectroscopy (XPS) spectra in Figure 5b and Figure S3, Supporting Information, and energy dispersive spectrometer (EDS)-mapping results in Figure S4, Supporting Information. For another, the Zn^{2+} ions in the V_6O_{13} interlayers inhibit the further Zn^{2+} intercalation because of the strong electrostatic interaction among the divalent Zn^{2+} ions when compared with the monovalent Li^+ and Na^+ ions.[6,26]

As elucidated in a previous study,[48] the kinetic of capacitive contribution can be obtained by a mathematical analysis on the CV profiles at different scan rates, as seen in **Figure 4**a. A power law links the scan rate with the current, which is $i = av^b$. Note that the equation can be converted as $\log(i) = \log(a) + b^*\log(v)$, from which we can reach a precise b value via a consequent mathematical fitting of the value of $\log(i)$ and $\log(v)$. As is well known, if the value of b is close to 0.5, we can summarize that the capacity is mainly contributed by the diffusion process, and if the b value is near 1, we can conclude that the capacity is dominated by the capacitive effect. In our study, by mathematically fitting the CV data, we acquired the relevant b values, as seen in Figure 4b. As shown in Figure 4d, with the increasing scan rates, the contribution ratio of capacitive effect shows an increasing trend. And at the applied scan rate of 1.0 mV s^{-1}, the contribution ratio of capacitive effect can reach up to 87%. The aforementioned pseudocapacitive result in Figure 4 indicates that the capacitive effect significantly contributes to the remarkable electrochemical behavior of the V_6O_{13} material.

Because the electrochemical performance of the Zn/V_6O_{13} system relies on the Zn^{2+} storage mechanism, we performed in our study electrochemical measurements such as ex situ X-ray powder diffraction (XRD), transmission electron microscopy (TEM), and XPS techniques to investigate the Zn^{2+} storage behavior. It can be clearly distinguished in **Figure 5**a that a series of new peaks at 7.92°, 16.13°, 24.35°, and 32.78° gradually appear during discharging and then reversibly disappear during charging, which indicates the formation of the highly reversible phase of $Zn_{0.25}V_2O_5{\cdot}H_2O$ (PDF#97-008-2328) upon Zn^{2+} insertion. Note that no similar phenomenon was detected in any previous reports on vanadium oxides in aqueous ZIB systems, which could be attributed to the unique open structure of V_6O_{13}.

© 2019 WILEY-VCH Verlag GmbH & Co. KGaA, Weinheim

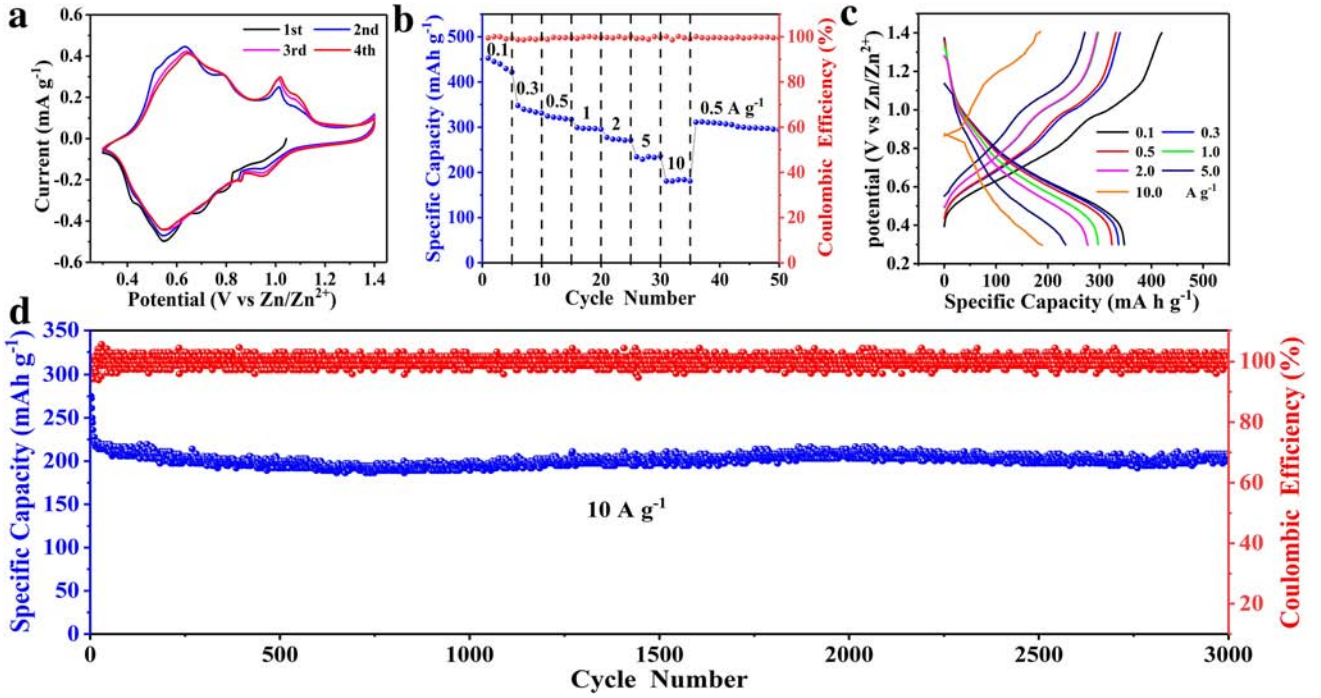

Figure 3. a) CV curves, b) rate performance, and c) corresponding discharge–charge curves at various rates of 0.1, 0.3, 0.5, 1.0, 2.0, 5.0, and 10.0 A g^{-1}; d) the cyclic performance at 10 A g^{-1} of V_6O_{13}.

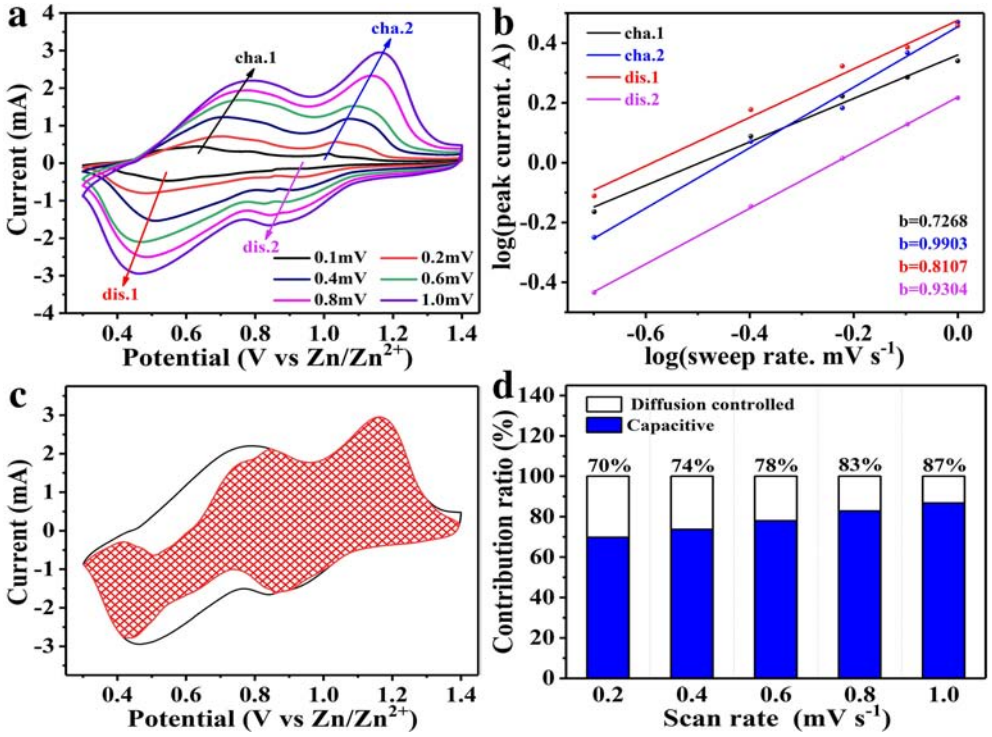

Figure 4. a) CV curves at various scan rates of 0.1–1.0 mV s^{-1}, b) fitting measurements at the redox peaks, c) the distribution of the capacitive effect and diffusion contribution at 1 mV s^{-1}, d) contribution ratio comparison of the capacitive effect and the diffusion process at various scan rates.

© 2019 WILEY-VCH Verlag GmbH & Co. KGaA, Weinheim

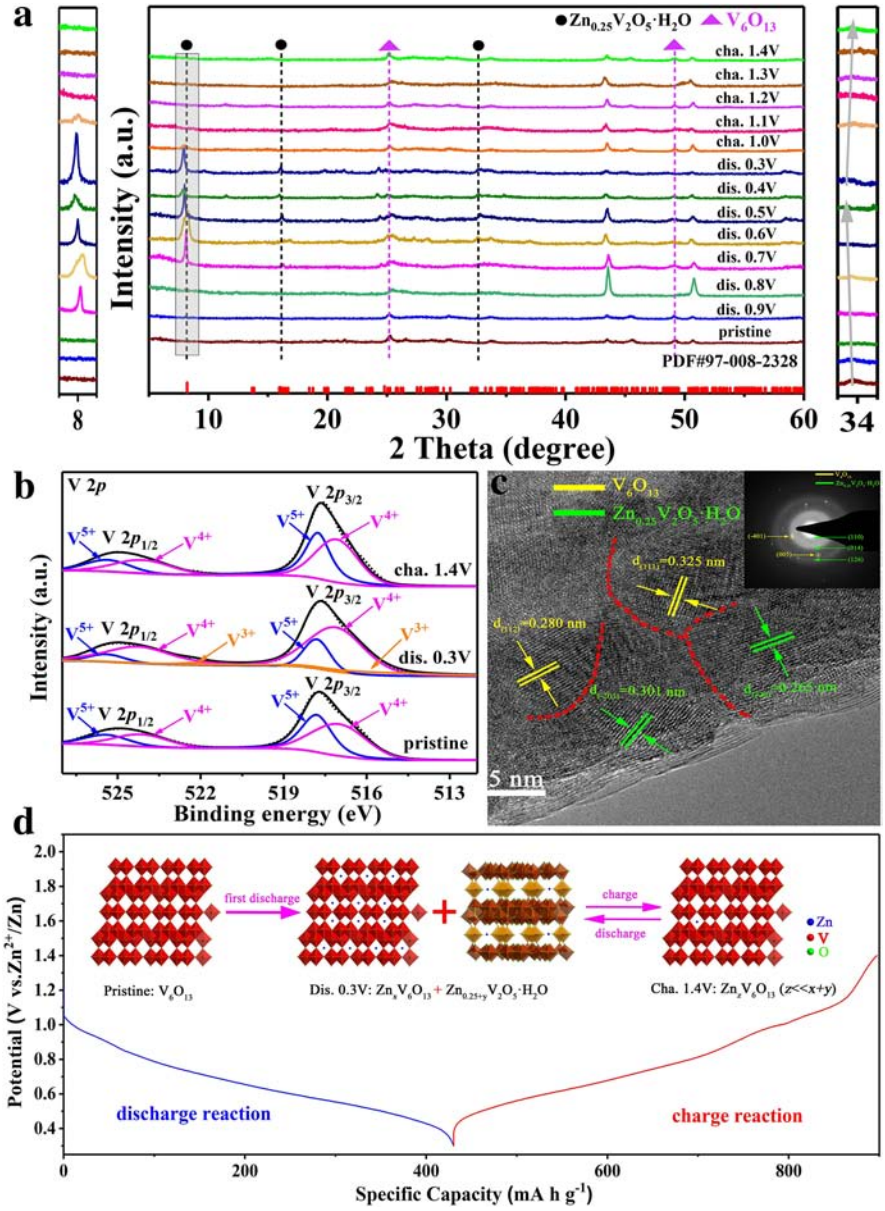

Figure 5. a) Ex situ XRD patterns at various discharge–charge states, b) XPS spectra of V, c) the HRTEM image with the corresponding SAED pattern at the fully discharged state, d) the schematic illustration of the highly reversible phase transition during the discharge–charge process of V_6O_{13}.

And the phase transition process was well illustrated to maintain great structural stability during cycling.[47,49] It can be reasonably speculated that the highly reversible phase transition process of $Zn_{0.25}V_2O_5{\cdot}H_2O$ is responsible for the brilliant electrochemical behavior of V_6O_{13}. On the one hand, the formation of $Zn_{0.25}V_2O_5{\cdot}H_2O$ enables the insertion of more Zn^{2+} ions into the host structure. On the other hand, this formation may result in numerous phase boundaries, leading to an enlarged interfacial contact area as well as providing more active sites,[50,51] which are conducive to storing numerous Zn^{2+} ions. In addition, the biphasic material may contribute to high electronic conductivity and pseudocapacitive effect,[50] leading to the fast ion diffusion kinetics. Moreover, the biphasic material with stepwise redox reactions can effectively reduce the solid-state diffusion and thus relieve the stress during the insertion of ions.[52–54] Remarkably, many zinc vanadates were demonstrated to exhibit superior electrochemical behavior as aqueous ZIB cathodes,[6,23,55] especially the $Zn_{0.25}V_2O_5{\cdot}nH_2O$ material reported by Nazar and coworkers,[6] whose study revealed that $Zn_{0.25}V_2O_5{\cdot}nH_2O$ can perform at a high capacity and demonstrate excellent long-term cyclic stability in virtue of its favorable structure. From that study, we can reasonably deduce that the formation of $Zn_{0.25}V_2O_5{\cdot}H_2O$ is markedly beneficial to boost the electrochemical behavior of the V_6O_{13} cathode.

To investigate the surface composition and valence states of V_6O_{13}, XPS profiles were collected at pristine, discharge,

© 2019 WILEY-VCH Verlag GmbH & Co. KGaA, Weinheim

and charge states, as shown in Figure 5b and Figure S3, Supporting Information. The V^{4+} and V^{3+} signals appear at the completely discharged state, which is due to the reduction of V^{5+} and V^{4+} along with the insertion of Zn^{2+}. At the fully charged state, most V^{4+} and V^{3+} are oxidized after being recharged to 1.4 V, accompanied by the extraction of Zn^{2+}. The high-resolution XPS spectra of the Zn element (shown in Figure S3, Supporting Information) also confirms the insertion/extraction of Zn^{2+} in the V_6O_{13} electrode. Furthermore, as shown in Figure 5c, the phases of V_6O_{13} and $Zn_{0.25}V_2O_5{\cdot}H_2O$ can be distinctly observed in the HRTEM image and the corresponding SAED pattern at the completely discharged state, which is in accordance with ex situ XRD results in Figure 5a. This result confirms the phase transition mechanism in the aqueous Zn/V_6O_{13} system.

It can be clearly detected in Figure 5a that the peak evolution located at 33.8° reveals the Zn^{2+} insertion/extraction process, i.e., the intercalated Zn^{2+} results in an enlarged lattice spacing, while subsequent deintercalation leads to the corresponding lattice recovery. Significantly, the high contents of mixed V^{4+}/V^{5+} are favorable to not only electrochemically store numerous Zn^{2+} ions but also enable the smooth valence evolution of vanadium. The energy storage mechanism of an aqueous Zn/V_6O_{13} cell is schematically illustrated in Figure 5d; i.e., the intercalated Zn^{2+} ions upon discharging not only enable the formation of $Zn_{0.25}V_2O_5{\cdot}H_2O$ but also locate at the empty sites of both V_6O_{13} and the newly formed $Zn_{0.25}V_2O_5{\cdot}H_2O$ phase. While in the subsequent charging, Zn^{2+} ions are extracted from the V_6O_{13} framework accompanied by the disappearance of $Zn_{0.25}V_2O_5{\cdot}H_2O$.

Based on the preceding discussion, the superior electrochemical properties of V_6O_{13} should be attributed to the following reasons: 1) the highly reversible phase transition of $Zn_{0.25}V_2O_5{\cdot}H_2O$ during the discharge/charge process enables V_6O_{13} to provide more sites for Zn^{2+} storage, thus resulting in a remarkable capacity; 2) V_6O_{13} possesses an extraordinary structural reversibility upon Zn^{2+} (de)intercalation, which is of great significance to long-term cyclability; 3) the high contents of mixed vanadium states of V^{4+}/V^{5+} and the metallic property of V_6O_{13} at room temperature enable superior electronic conductivity and ion diffusion coefficient, leading to the fast Zn^{2+} transportation;[37,39] and 4) the pseudocapacitive effect (Figure 4) is also responsible for the excellent rate capability and cycling stability. Moreover, the open structure, along with the high contents of mixed vanadium states of V^{4+}/V^{5+}, enables V_6O_{13} to buffer the volume variation and valence evolution from Zn^{2+} (de)intercalation, thus stabilizing the host structure.

3. Conclusion

In conclusion, we detected the phase transition mechanism based on the aqueous Zn/V_6O_{13} cell. Benefiting from the second phase formation (i.e., $Zn_{0.25}V_2O_5{\cdot}H_2O$), an advantageous structure with mixed-valance states of V^{4+}/V^{5+}, V_6O_{13} can perform at a high capacity and demonstrate long-term cycling stability at high rates, rendering it a promising cathode in future aqueous ZIBs. The investigation of V_6O_{13} provides a new perspective to understand the energy storage mechanism and design novel cathode materials with the brilliant electrochemical behavior of aqueous ZIBs.

4. Experimental Section

Material Synthesis: V_6O_{13}. All the reactants were used as received without further purification. In the typical process, 0.9 g of V_2O_5 was dissolved in the mixed solution of 10 mL ethanol and 30 mL deionized water. After being magnetically stirred at room temperature for 1 h, the solution was transferred into 50 mL Teflon-lined autoclave and heated at 180 °C for 12 h. Then the resultant solution was washed with ethanol for several times and dried at 75 °C for 12 h during vacuum atmosphere to obtain V_6O_{13}.

VO_2. V_2O_5 (1.2 g) and $H_2C_2O_4{\cdot}H_2O$ (1.8 g) were dissolved in 40 mL of deionized water. After stirred at 75 °C for 1 h, the solution was transferred into 50 mL Teflon-lined autoclave and heated at 180 °C for 3 h. Then the resultant solution was washed with ethanol for several times and dried at 70 °C overnight during vacuum atmosphere to obtain VO_2.

V_2O_5. V_2O_5 (1.2 g) and $H_2C_2O_4{\cdot}2H_2O$ (2.562 g) were dissolved in 40 mL of deionized water under vigorous stirring at 80 °C for several hours until a clear-blue solution was formed. The as-prepared solution (3 mL) was then added into a 50 mL Teflon container pre-filled with 30 mL of isopropanol. After the solution was stirred for 20 min, the container was sealed in a steel autoclave and kept in an electrical oven at 200 °C for 2.5 h. After cooling down naturally, the precipitate was collected by centrifugation and washed with pure ethanol for three times. After calculation in air at 350 °C for 2 h with a heating rate of 1 °C min^{-1}, V_2O_5 was obtained.

Material Characterization: The XRD was used to identify the as-prepared V_6O_{13} product. Scanning electron microscopy (SEM) and TEM were used to obtain the microcosmic crystal morphologies and sizes. XPS spectra were performed using an ESCALAB 250Xi X-ray photoelectron spectrometer (Thermo Fisher).

Electrochemical Measurements: The assembly of coin cells is illustrated in our previous study.[16] The specific capacity and rate capability of V_6O_{13} product were measured using Land battery tester during the voltage scale of 0.3–1.4 V (vs Zn/Zn^{2+}). In addition, the electrochemical workstation was used to characterize the CV curves at a scan rate of 0.1 mV s^{-1} during the voltage scale of 0.3–1.4 V (vs Zn/Zn^{2+}).

Supporting Information

Supporting Information is available from the Wiley Online Library or from the author.

Acknowledgements

This work was supported by National Natural Science Foundation of China (Grant no. 51802356, 51872334 and 51572299), Innovation-Driven Project of Central South University (No. 2018CX004), and the Research Support Fund of the Collaborative Innovation Center of Manganese-Zinc-Vanadium Industrial Technology in Hunan Province (No. 201809).

Conflict of Interest

The authors declare no conflict of interest.

Keywords

aqueous zinc-ion batteries, cathodes, energy storage mechanisms, phase transitions, V_6O_{13}

Received: January 3, 2019
Revised: January 30, 2019
Published online: April 12, 2019

© 2019 WILEY-VCH Verlag GmbH & Co. KGaA, Weinheim

[1] J. M. Tarascon, M. Armand, *Nature* **2001**, *414*, 359.
[2] V. Etacheri, R. Marom, R. Elazari, G. Salitra, D. Aurbach, *Energy Environ. Sci.* **2011**, *4*, 3243.
[3] J. B. Goodenough, Y. Kim, *Chem. Mater.* **2010**, *22*, 587.
[4] R. Chen, Z. Wang, Z. Chen, P. Wang, G. Fang, J. Zhou, X. Tan, S. Liang, *J. Alloys Compd.* **2019**, *772*, 852.
[5] T. Chen, J. Zhou, G. Fang, Y. Tang, X. Tan, A. Pan, S. Liang, *ACS Sustainable Chem. Eng.* **2018**, *6*, 7250.
[6] D. Kundu, B. D. Adams, V. Duffort, S. H. Vajargah, L. F. Nazar, *Nat. Energy* **2016**, *1*, 16119.
[7] F. Wang, O. Borodin, T. Gao, X. Fan, W. Sun, F. Han, A. Faraone, J. A. Dura, K. Xu, C. Wang, *Nat. Mater.* **2018**, *17*, 543.
[8] L. Zhang, L. Chen, X. Zhou, Z. Liu, *Adv. Energy Mater.* **2014**, *5*, 1400930.
[9] G. Fang, J. Zhou, A. Pan, S. Liang, *ACS Energy Lett.* **2018**, *3*, 2480.
[10] D. Kundu, S. Hosseini Vajargah, L. Wan, B. Adams, D. Prendergast, L. F. Nazar, *Energy Environ. Sci.* **2018**, *11*, 881.
[11] J. Ding, Z. Du, L. Gu, B. Li, L. Wang, S. Wang, Y. Gong, S. Yang, *Adv. Mater.* **2018**, *30*, 1800762.
[12] M. Yan, P. He, Y. Chen, S. Wang, Q. Wei, K. Zhao, X. Xu, Q. An, Y. Shuang, Y. Shao, K. T. Mueller, L. Mai, J. Liu, J. Yang, *Adv. Mater.* **2018**, *30*, 1703725.
[13] Y. Cai, F. Liu, Z. Luo, G. Fang, J. Zhou, A. Pan, S. Liang, *Energy Storage Mater.* **2018**, *13*, 168.
[14] V. Soundharrajan, B. Sambandam, S. Kim, M. H. Alfaruqi, D. Y. Putro, J. Jo, S. Kim, V. Mathew, Y. K. Sun, J. Kim, *Nano Lett.* **2018**, *18*, 2402.
[15] F. Wan, L. Zhang, X. Dai, X. Wang, Z. Niu, J. Chen, *Nat. Commun.* **2018**, *9*, 1656.
[16] J. Zhou, L. Shan, Z. Wu, X. Guo, G. Fang, S. Liang, *Chem. Commun.* **2018**, *54*, 4457.
[17] C. Xu, B. Li, H. Du, F. Kang, *Angew. Chem. Int. Ed.* **2012**, *51*, 933.
[18] N. Zhang, F. Cheng, J. Liu, L. Wang, X. Long, X. Liu, F. Li, J. Chen, *Nat. Commun.* **2017**, *8*, 405.
[19] H. Pan, Y. Shao, P. Yan, Y. Cheng, K. S. Han, Z. Nie, C. Wang, J. Yang, X. Li, P. Bhattacharya, K. T. Mueller, J. Liu, *Nat. Energy* **2016**, *1*, 16039.
[20] B. Lee, C. S. Yoon, H. R. Lee, K. Y. Chung, B. W. Cho, S. H. Oh, *Sci. Rep.* **2014**, *4*, 6066.
[21] W. Sun, F. Wang, S. Hou, C. Yang, X. Fan, Z. Ma, T. Gao, F. Han, R. Hu, M. Zhu, C. Wang, *J. Am. Chem. Soc.* **2017**, *139*, 9775.
[22] M. H. Alfaruqi, V. Mathew, J. Gim, S. Kim, J. Song, J. P. Baboo, S. H. Choi, J. Kim, *Chem. Mater.* **2015**, *27*, 3609.
[23] C. Xia, J. Guo, Y. Lei, H. Liang, C. Zhao, H. N. Alshareef, *Adv. Mater.* **2018**, *30*, 1705580.
[24] P. He, G. Zhang, X. Liao, M. Yan, X. Xu, Q. An, J. Liu, L. Mai, *Adv. Energy Mater.* **2018**, *8*, 1702463.
[25] Z. Peng, Q. Wei, S. Tan, P. He, W. Luo, Q. An, L. Mai, *Chem. Commun.* **2018**, *54*, 4041.
[26] C. Xia, J. Guo, P. Li, X. Zhang, N. Alshareef Husam, *Angew. Chem. Int. Ed.* **2018**, *57*, 3943.
[27] X. Guo, G. Fang, W. Zhang, J. Zhou, L. Shan, L. Wang, C. Wang, T. Lin, Y. Tang, S. Liang, *Adv. Energy Mater.* **2018**, *8*, 1801819.
[28] Y. Yang, Y. Tang, G. Fang, L. Shan, J. Guo, W. Zhang, C. Wang, L. Wang, J. Zhou, S. Liang, *Energy Environ. Sci.* **2018**, *11*, 3157.
[29] B. Tang, J. Zhou, G. Fang, F. Liu, C. Zhu, C. Wang, A. Pan, S. Liang, *J. Mater. Chem. A* **2019**, *7*, 940.
[30] P. Hu, M. Yan, T. Zhu, X. Wang, X. Wei, J. Li, L. Zhou, Z. Li, L. Chen, L. Mai, *ACS Appl. Mater. Interfaces* **2017**, *9*, 42717.
[31] X. Li, C. Liu, C. Zhang, H. Fu, X. Nan, W. Ma, Z. Li, K. Wang, H. Wu, G. Cao, *ACS Appl. Mater. Interfaces* **2016**, *8*, 24629.
[32] B. Yan, X. Li, Z. Bai, Y. Zhao, L. Dong, X. Song, D. Li, C. Langford, X. Sun, *Nano Energy* **2016**, *24*, 32.
[33] Y. Lu, J. Wu, J. Liu, M. Lei, S. Tang, P. Lu, L. Yang, H. Yang, Q. Yang, *ACS Appl. Mater. Interface* **2015**, *7*, 17433.
[34] Q. Liu, G. Tan, P. Wang, S. C. Abeyweera, D. Zhang, Y. Rong, Y. A. Wu, J. Lu, C.-J. Sun, Y. Ren, Y. Liu, R. T. Muehleisen, L. B. Guzowski, J. Li, X. Xiao, Y. Sun, *Nano Energy* **2017**, *36*, 197.
[35] N. A. Chernova, M. Roppolo, A. C. Dillon, M. S. Whittingham, *J. Mater. Chem.* **2009**, *19*, 2526.
[36] H. Y. K. H. Xue, Y. M. Zhou, G. Li, T. A. Skotheim, H. S. Lee, X. Q. Yang, J. McBreen, *J. Electrochem. Soc.* **1993**, *140*, 3413.
[37] Y. L. Ding, Y. Wen, C. Wu, P. A. van Aken, J. Maier, Y. Yu, *Nano Lett.* **2015**, *15*, 1388.
[38] M. Menetrier, A. Levasseur, C. Delmas, *Mater. Sci. Eng. B* **1989**, *3*, 103.
[39] K. West, B. Zachau-Christiansen, T. Jacobsen, *Electrochim. Acta* **1983**, *28*, 1829.
[40] H. Chen, C. Chen, Y. Liu, X. Zhao, N. Ananth, B. Zheng, L. Peng, T. Huang, W. Gao, C. Gao, *Adv. Energy Mater.* **2017**, *7*, 1700051.
[41] S. S. Zhang, K. Xu, T. R. Jow, *Electrochim. Acta* **2006**, *51*, 1636.
[42] D. Wang, Q. Wei, J. Sheng, P. Hu, M. Yan, R. Sun, X. Xu, Q. An, L. Mai, *Phys. Chem. Chem. Phys.* **2016**, *18*, 12074.
[43] A. Petric, H. Ling, *J. Am. Ceram. Soc.* **2007**, *90*, 1515.
[44] J. Xu, M. Wang, N. P. Wickramaratne, M. Jaroniec, S. Dou, L. Dai, *Adv. Mater.* **2015**, *27*, 2042.
[45] W. Ren, H. Zhang, C. Guan, C. Cheng, *Adv. Funct. Mater.* **2017**, *27*, 1702116.
[46] Y. Fu, Q. Wei, G. Zhang, X. Wang, J. Zhang, Y. Hu, D. Wang, L. Zuin, T. Zhou, Y. Wu, S. Sun, *Adv. Energy Mater.* **2018**, *8*, 1801445.
[47] L. Shan, Y. Yang, W. Zhang, H. Chen, G. Fang, J. Zhou, S. Liang, *Energy Storage Mater.* **2019**, *18*, 10.
[48] W. Meng, R. Pigliapochi, P. M. Bayley, O. Pecher, M. W. Gaultois, I. D. Seymour, H.-P. Liang, W. Xu, K. M. Wiaderek, K. W. Chapman, C. P. Grey, *Chem. Mater.* **2017**, *29*, 5513.
[49] W. Meng, R. Pigliapochi, P. M. Bayley, O. Pecher, M. W. Gaultois, I. D. Seymour, H.-P. Liang, W. Xu, K. M. Wiaderek, K. W. Chapman, C. P. Grey, *Chem. Mater.* **2017**, *29*, 5513.
[50] Q. Wu, J. Xu, X. Yang, F. Lu, S. He, J. Yang, H. J. Fan, M. Wu, *Adv. Energy Mater.* **2015**, *5*, 1401756.
[51] S. Wang, Y. Yang, W. Quan, Y. Hong, Z. Zhang, Z. Tang, J. Li, *Nano Energy* **2017**, *32*, 294.
[52] S. Dong, C. Li, X. Ge, Z. Li, X. Miao, L. Yin, *ACS Nano* **2017**, *11*, 6474.
[53] G. Fang, J. Zhou, Y. Cai, S. Liu, X. Tan, A. Pan, S. Liang, *J. Mater. Chem. A* **2017**, *5*, 13983.
[54] G. Fang, Z. Wu, J. Zhou, C. Zhu, X. Cao, T. Lin, Y. Chen, C. Wang, A. Pan, S. Liang, *Adv. Energy Mater.* **2018**, *8*, 1703155.
[55] B. Sambandam, V. Soundharrajan, S. Kim, M. H. Alfaruqi, J. Jo, S. Kim, V. Mathew, Y.-K. Sun, J. Kim, *J. Mater. Chem. A* **2018**, *6*, 3850.

© 2019 WILEY-VCH Verlag GmbH & Co. KGaA, Weinheim